ACS APPLIED MATERIALS & INTERFACES

Research Article

www.acsami.org

Platelet CMK-5 as an Excellent Mesoporous Carbon to Enhance the Pseudocapacitance of Polyaniline

Zhibin Lei,*[,†] Xiuxia Sun,[†] Huanjing Wang,[†] Zonghuai Liu,[†] and X. S. Zhao*[,‡]

[†]School of Materials Science and Engineering, Shaanxi Normal University, 199 South Chang'an Road, Xi'an, Shaanxi, 710062, China

[‡]School of Chemical Engineering, Faculty of Engineering, Architecture and Information Technology, The University of Queensland, St Lucia, Brisbane, QLD, 4072, Australia

Supporting Information

ABSTRACT: A high-performance supercapacitor electrode consisting of platelet ordered mesoporous carbon CMK-5 and polyaniline (PANi) was prepared by chemical oxidative polymerization of aniline in the presence of CMK-5. The PANi with uniform size of 2−5 nm was primarily confined in the mesochannels of CMK-5 at low PANi loadings (40 and 51 wt %), whereas at a high loading of 64 wt %, additional PANi thin films with thicknesses of 5−10 nm were coated on the surface of the CMK-5 particles. Such CMK-5-PANi composites afforded a high electrochemical active surface area for surface Faradic redox reactions, leading to a more than 50% utilization efficiency when considering the theoretical capacitance of PANi of about 2000 F/g. As a result, a specific capacitance of 803 F/g and an energy density of 27.4 Wh/kg were achieved for CMK-5-PANi composite electrode with 64 wt % PANi, showing substantial improvement as compared with symmetric capacitors configured with CMK-5 electrodes (10.1 Wh/kg) or pure PANi electrodes (16.4 Wh/kg). Moreover, an excellent rate capability and a substantially enhanced electrochemical stability with 81% capacitance retention as compared with 68% of pure PANi were also observed over 1000 charge−discharge cycles at a constant current density of 4.0 A/g.

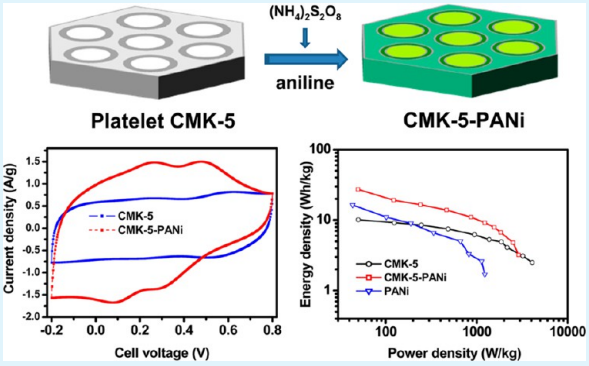

KEYWORDS: *mesoporous carbon CMK-5, polyaniline, composite electrode, pseudocapacitance*

1. INTRODUCTION

Supercapacitors, also known as electrochemical capacitors, have received great research interest during the past several years because of their properties like high power capability, long cycle life, and fast charging/discharging rate.[1,2] These characteristics make the supercapacitor one of the promising energy storage systems that could find wide applications in portable electronic devices or as auxiliary devices for high power sources.[3] Depending on the energy storage mechanisms, supercapacitors can be classified as electrochemical double-layer (EDL) capacitors and pseudocapacitors.[2,4] The EDL capacitor stores energy through electrostatic adsorption of electrolyte ions at the electrode/electrolyte interface. Various carbon-based materials including CNTs, graphene, and activated carbon with controlled microtextures and tailored physicochemical properties have been widely investigated as EDL supercapacitor electrode.[5] The high surface area, good electronic conductivity, and excellent electrochemical stability offer these carbon-based supercapacitors the excellent power performance and superior cycling stability.[6−8] However, these carbon-based supercapacitors usually store less energy than 10 Wh/kg in aqueous electrolyte due to the limited surface area available for ion adsorption.[9] On the other hand, the pseudocapacitor accumulates charges chemically through fast and reversible surface Faradic redox reactions between the surface layer of electrode and electrolyte. Most metal oxides and conducting polymers store charge by this pseudocapacitance mechanism. Given that a chemical redox reaction is usually involved in the charge-storage process, the energy stored in the pseudocapacitor is much higher than that in the EDL capacitor. Thus, these pseudocapacitive electrodes have great potentials for high-energy supercapacitors.[10−14] However, due to the kinetically slow charge transfer nature, the rate capability of the pseudocapacitor is generally inferior to the EDL capacitor. Moreover, the poor cycling stability and the narrow working potential windows along with the low electrical conductivity of most metal oxides largely restrict their applications in the supercapacitor industry.[15−18]

Conducting polymers represent an important family of pseudocapacitive electrode materials for supercapacitors. Among various conducting polymers, polyaniline (PANi) has received great attention because of its low cost, high capacitance value, good environmental stability, and unusual doping/dedoping chemistry.[19] However, the low electronic conductivity and mechanical degradation due to swelling and shrinkage during charging−discharging processes are the key

Received: May 13, 2013
Accepted: July 12, 2013
Published: July 12, 2013

   dx.doi.org/10.1021/am4018016 | ACS Appl. Mater. Interfaces 2013, 5, 7501−7508

problems. A common strategy to overcome these issues is to incorporate PANi into carbon-based materials to prepare composite electrodes.[20−23] Such composite electrodes integrate the excellent electrical conductivity and good mechanical properties of the carbon materials with the high pseudocapacitance of PANi, thus allowing an enhanced electrocapacitive performance. Given that the pseudocapacitance of PANi comes from the surface Faradic redox reaction, PANi with a large electrochemical active surface area would be highly desirable to maximize its utilization efficiency.[24,25] Although the highly conductive CNTs and graphene have been applied as the carbon matrix for growth of PANi with controlled nanostructure, the low external surface of CNTs and the easily aggregated graphene sheets hardly provide a high contact interface between PANi and electrolyte.[26−28] Therefore, exploration of porous carbons with a high surface area and open inner channels is of great significance in improving the utilization efficiency of PANi for electrochemical energy storage.

Herein, platelet mesoporous carbon CMK-5 with high surface area and small particle size was adopted as a carbon material for PANi incorporation. The platelet CMK-5 matrix has a number of advantages over conventional activated carbon[29] and ordered mesoporous carbon CMK-3[30,31] in view of its high surface area, bimodal pore size, and short and straight mesochannels, which greatly prompt ion diffusion and maximize the utilization efficiency of PANi for Faradic redox reaction. As a result, a CMK-5-PANi composite electrode with 64 wt % PANi exhibited a high specific capacitance up to 803 F/g in 2.0 mol/L aqueous H_2SO_4 electrolyte, showing substantial improvement as compared with 293 F/g of CMK-5 and 629 F/g of pure PANi. Moreover, the CMK-5-PANi composite electrode also exhibited remarkable rate performance and excellent cycling performance, with 81% capacitance retention after 1000 charge−discharge cycles.

2. EXPERIMENTAL SECTION

Sample Preparation. Platelet mesoporous carbon CMK-5 was prepared by using the chemical vapor deposition method with ferrocene as the carbon precursor and platelet mesoporous SBA-15 as sacrificial template as described previously.[32] To improve the graphitization of CMK-5, the silica/carbon composite was annealed at 800 °C for 90 min before etching in 10% HF solution. CMK-5 was collected by filtration, followed by washing with copious deionized water and ethanol, and drying at 80 °C.

Incorporating PANi to platelet CMK-5 was conducted by oxidative polymerization of aniline in the presence of CMK-5. Typically, a given amount of aniline (25, 50, and 75 μL) was added to 20 mL of 2.0 mol/L HCl aqueous solution, followed by addition of 30 mg of CMK-5 into the solution. Then, ammonium persulfate (APS) with a molar ratio of aniline/APS of 1.5 was dissolved in 10 mL of 2.0 mol/L HCL aqueous solution and then added to the aniline solution under vigorous stirring. The polymerization was carried out at room temperature (25 °C) for 12 h. The final products were filtrated and rinsed with deionized water and ethanol for several times. The content of PANi in the composite was calculated by measuring the mass difference before and after polymerization reaction. The present recipes yielded CMK-5-PANi composites with PANi mass contents of 40, 51, and 64 wt %, respectively, which were denoted as CMK-5-PANi-x with x representing the mass percentage of PANi in the composite. A pure PANi sample was prepared under the identical conditions except that mesoporous carbon CMK-5 was not included in the solution.

Characterization. Nitrogen adsorption/desorption isotherms were measured at 77 K on Nova 1000 series. Samples were degassed at 180 °C for 6 h prior to the measurement. The specific surface areas of the samples were calculated using the Brunauer−Emmett−Teller (BET) method with the adsorption data at the relative pressure (P/P_o) range of 0.05−0.2. Total pore volumes were calculated at P/P_o = 0.99. The pore size distribution (PSD) curves were derived from the adsorption branch using the Barrett−Joyner−Halenda (BJH) equation. The morphology of the samples was observed on JEOL JSF-6700F field-emission scanning electron microscopy (FESEM). High-resolution transmission electron microscopy (HRTEM) was performed on a field-emission JEOL JEM-2100F at an acceleration voltage of 200 kV. The Fourier transform infrared (FT-IR) spectra of the samples were measured on a Shimadzu Prestige-21 FT-IR spectrophotometer. X-ray photoelectron spectroscopy (XPS) spectra were collected on an AXIS Ultra spectrometer (Kratos Analytical Ltd.) using a monochromatized Al Kα X-ray source (1486.71 eV).

Electrochemical Measurement. The working electrode was prepared by mixing an active material (90 wt %), carbon black (5 wt %), and polytetrafluoroethylene (5 wt %) in water. The slurry of the mixture was then painted between two pieces of stainless steel mesh with area of 1.0 cm^2 and pressed under a pressure of 500 kg/cm^2. The mass loading of the active material was typically about 5.0 mg/cm^2. A supercapacitor was configured symmetrically with two working electrodes, which were separated by a membrane filter (Durapore). A stainless steel plate was used as current collector, and 2.0 mol/L aqueous H_2SO_4 was applied as the electrolyte. The performance of the supercapacitor cell was tested by cyclic voltammetry (CV), galvanostatic charge−discharge, and electrochemical impedance spectroscopy (EIS) on an Autolab PGSTAT302N electrochemical workstation. The voltage range for the CV and galvanostatic charge−discharge measurements varied from −0.2 to 0.8 V, while the current density for the galvanostatic measurement varied from 0.1 to 10 A/g. EIS data were collected with an amplitude of 10 mV in the frequency range of 100 kHz to 4 mHz. The specific capacitance of a single electrode was calculated from the galvanostatic discharge process according to the following equation: $C_{single} = 4 \times I \times \Delta t/(\Delta V \times m)$,[33] where I is the discharge current (A), Δt is the discharge time (s), ΔV is the voltage variation during the discharge process, and m is the total mass of the active material in both electrodes (g).

3. RESULTS AND DISCUSSION

Figure 1a shows the FESEM image of mesoporous carbon CMK-5 product. It is seen that the carbon particles exhibited a

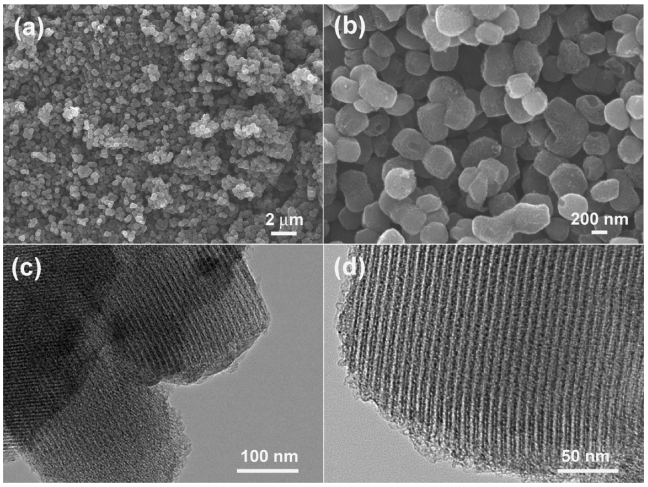

Figure 1. FESEM (a, b) and TEM (c, d) images of platelet CMK-5 with different magnifications.

platelet morphology, similar to that of the SBA-15 template (not shown). A close examination showed that most of the individual CMK-5 particles had a primary platelet size of ~500 nm (Figure 1b). The surface of these carbons look rough with some of cavities being clearly seen. Because the pyrolysis of ferrocene yields both carbon and Fe particles,[34] these cavities

were most likely left behind by the dissolved Fe nanoparticles during etching of SBA-15 with HF aqueous solution. The porous microstructure of the CMK-5 was confirmed by HRTEM. As displayed in Figure 1c,d, each carbon platelet is composed of two types of mesopores, which were generated by insufficient filling of SBA-15 mesopores with carbon and the dissolution of SBA-15 silica with aqueous HF solution, respectively.[34] The nanopipes microstructure of the carbon platelet revealed that these carbon platelets are characteristic of ordered mesoporous carbon CMK-5. On the other hand, the strongest (110) reflection at $2\theta = 1.6°$ of the carbon product (Figure S1, Supporting Information) in contrast with the strongest (100) peak of SBA-15 at $2\theta = 0.9°$ confirmed the formation of mesoporous carbon CMK-5.[34] The N_2 isotherms of CMK-5 are of classical type IV with a H1 hysteresis loop at relative pressures of 0.4−0.7 (Figure 2a), indicating the

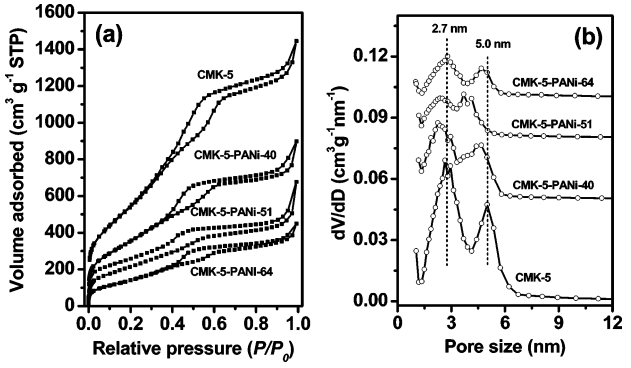

Figure 2. N_2 adsorption isotherms (a) and BJH pore size distribution curves (b) of platelet CMK-5 and CMK-5-PANi composites.

presence of uniform mesopores in the CMK-5 product. The narrow pore size distribution (Figure 2b) with two peaks occurring at 2.7 and 5.0 nm is in good agreement with the small-angle XRD and TEM results. With the unique structural properties of bimodal pore size, the CMK-5 platelet exhibited a specific surface area as high as 1987 m^2/g and a total pore volume up to 2.24 cm^3/g (Table 1).

Incorporating PANi to CMK-5 was accomplished by oxidative polymerization of aniline in the presence of CMK-5. Figure 3a displays the FT-IR spectra of CMK-5-PANi composite. The CMK-5 did not show characteristic absorption bands in the measured wavelength range. The CMK-5-PANi composite presented absorption bands similar to that of the pure PANi. The two distinct peaks appearing at 1304 and 1146 cm^{-1} are related to the C−N stretching modes and the C−H in-plane bending mode of pernigraniline, respectively.[35] The two strong bands at 1500 and 1579 cm^{-1} can be ascribed to the C═C stretching vibration modes of benzenoid and quinonoid rings of PANi, respectively.[36] The survey XPS spectrum of the CMK-5-PANi-64 composite is shown in Figure 3b. The 1s signals of elements N, O, and C are clearly seen. The deconvoluted N 1s spectrum shows three distinct peaks centered at 398.4, 399.3, and 400.9 eV, which correspond to the quinonoid imine, the benzenoid amine, and the nitrogen cationic radical of PANi molecular, repectively.[24] These results indicate the successful polymerization of PANi.

The macroscopic morphologies of the composites were examined by FESEM, and the representative images are shown in Figure 4. In spite of different amounts of PANi included, the CMK-5-PANi composite continued to have similar morphology as that of CMK-5. After careful comparison, it is found that most of the cavities on the pristine CMK-5 platelets disappeared. Instead, its surface became smoother (inset in Figure 4a) as compared with that of pristine CMK-5, suggesting the formation of PANi layer on the external surface of CMK-5 platelets. Figure 5 shows the TEM images of the CMK-5-PANi composites. It is seen that many PANi particles with sizes of 2−5 nm were confined in the mesochannels of the peripheral domain of CMK-5 platelet (see arrows in Figure 5b,c). At a high PANi loading of 64 wt %, additional thin films of PANi with thicknesses of about 5−10 nm were coated on the surface of the CMK-5 (see arrow in Figure 5d). No bulky PANi was observed from the CMK-5-PANi composites, suggesting a high dispersion of PANi on the CMK-5. In addition, the presence of the (110) reflection from the small-angle XRD pattern (Figure S1, Supporting Information) demonstrated that the incorporation of PANi did not destroy the long-range ordering of CMK-5. It is worth noting that both the PANi nanoparticles and thin films are of great significance in improving its utilization efficiency because only the surface layer of PANi is involved in Faradic redox reaction. Moreover, these confined PANi particles could also avoid a large volume change during charging/discharging processes.

N_2 adsorption of the CMK-5-PANi composite was measured and compared with that of CMK-5. As shown in Figure 2a, the CMK-5-PANi composites showed similar isotherm to CMK-5 except a distinctly reduced N_2 uptake, suggesting a more decreased specific surface area and reduced pore volume due to PANi incorporation (Table 1). The pore size distribution curves displayed bimodal pore sizes with the larger one

Table 1. Physicochemical Properties of CMK-5-PANi Composites and Their Capacitive Performances

samples	S_{BET} (m^2/g)	V_{total} (cm^3/g)	content of PANi (wt %)	ESR[b] (Ohm)	specific capacitance[a] (F/g)		energy density[c] (Wh/kg)
					composite	PANi	
CMK-5	1987	2.24	0	0.027	293		10.1
CMK-5-PANi-40	1288	1.39	40	0.034	386	525	13.2
CMK-5-PANi-51	777	1.05	51	0.039	553	803	18.9
CMK-5-PANi-64	520	0.70	64	0.050	803	1090	27.4
PANi	63	0.46	100	0.124	629	629	16.4

[a]The specific capacitance of the single electrode was recalculated on the basis of the galvanostatic discharge process of symmetric supercapacitor at current density of 0.1 A/g. The specific capacitance of PANi was derived from $C_{PANi} = [C_{composite} - C_{CMK\text{-}5} \times (1 - x)]/x$; where $C_{composite}$ and $C_{CMK\text{-}5}$ were the specific capacitance of composite and pure CMK-5 (293 F/g), respectively, whereas x represented the mass percentage of PANi in the composite. [b]ESR was calculated from the slope of the linear correlation between the voltage and discharge current density. [c]Energy density was obtained at current density of 0.1 A/g.

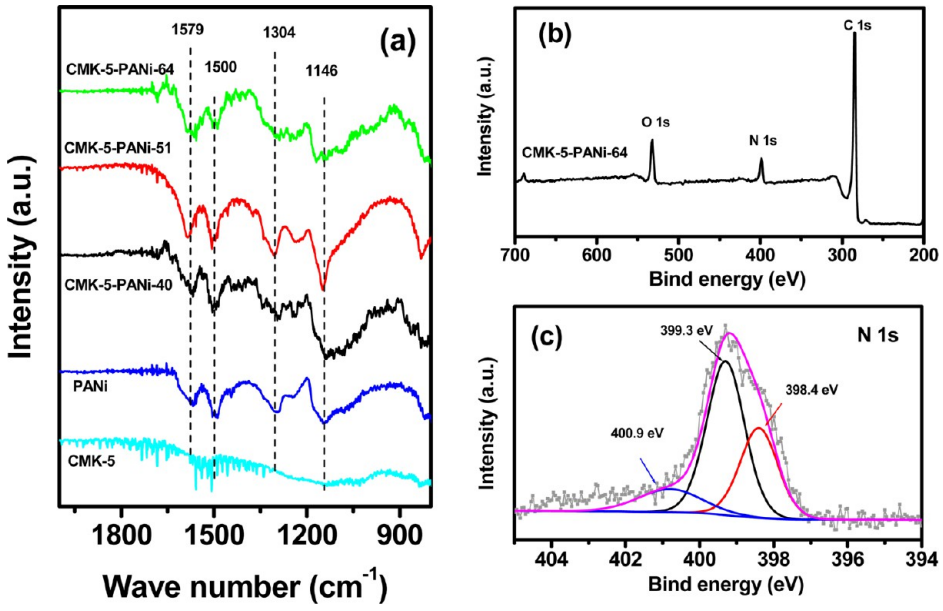

Figure 3. FT-IR spectra of platelet CMK-5, PANi, and CMK-5-PANi composites (a), survey XPS (b) and N 1s XPS spectrum (c) of CMK-5-PANi-64 composite.

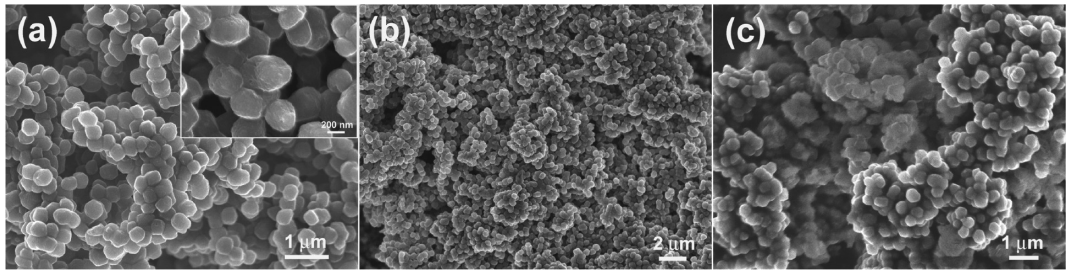

Figure 4. FESEM images of CMK-5-PANi-40 (a), CMK-5-PANi-51 (b), and CMK-5-PANi-64 (c). The inset in panel (a) shows the high-magnification FESEM images of CMK-5-PANi-40.

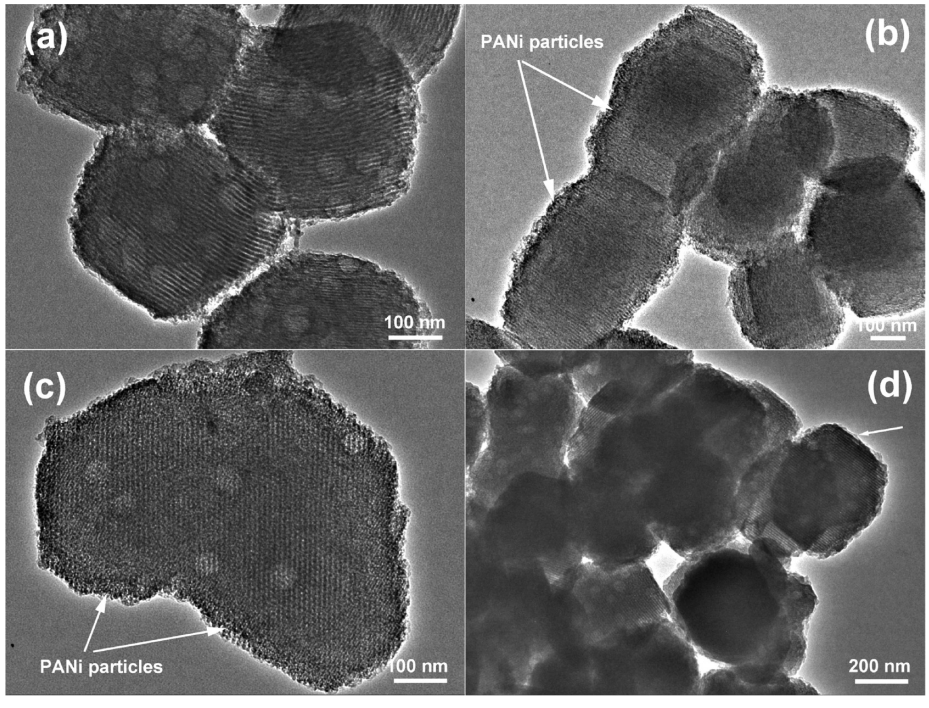

Figure 5. TEM images of CMK-5-PANi-40 (a), CMK-5-PANi-51 (b, c), and CMK-5-PANi-64 (d).

dx.doi.org/10.1021/am4018016 | ACS Appl. Mater. Interfaces 2013, 5, 7501−7508

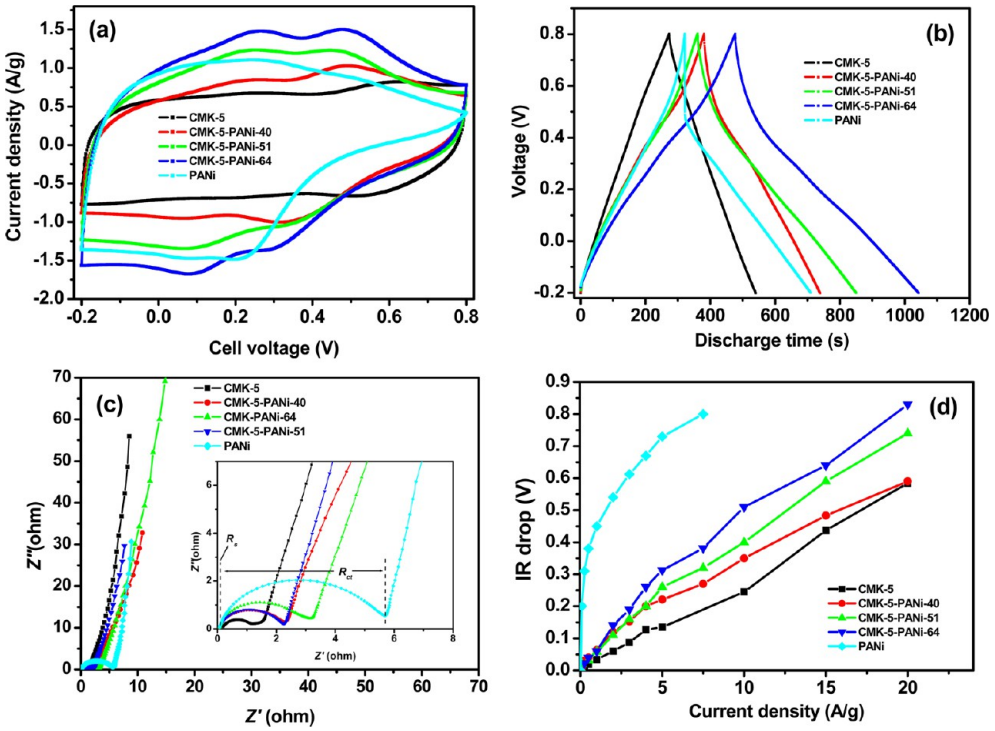

Figure 6. (a) CV profiles at 5 mV/s, (b) galvanostatic charge−discharge curves at current density of 0.25 A/g, (c) Nyquist plots, and (d) variation of IR drop against current density for various electrode materials. Data obtained from a two-electrode cell with 2.0 mol/L H_2SO_4 as the electrolyte.

gradually shifting toward a lower value (Figure 2b). This shift suggested a reduced pore size due to the existence of PANi particles in the mesochannels, consistent with the TEM results (Figure 5). As a result, both specific surface area and pore volume showed a continuous decrease with the increase of PANi content (Table 1). It should be noted that the CMK-5-PANi composites still had a high surface area, for example, 520 m^2/g for sample CMK-5-PANi-64.

The electrochemical properties of the CMK-5-PANi composites with different contents of PANi were evaluated by CV and galvanostatic charge−discharge in a two-electrode configuration. Figure 6a compares the CV curves of different electrodes at a scan rate of 5 mV/s in 2.0 mol/L H_2SO_4 aqueous electrolyte. The CMK-5 electrode showed a rectangular CV behavior, characteristic of double layer capacitance arisen from charge accumulation at the electrode/electrolyte interface. The CMK-5-PANi composites showed two pairs of redox waves, with the first oxidation peak at 0.25 V, corresponding to the structure conversion of PANi from leucoemeraldine to emeraldine, and the second peak at 0.45 V, attributed to the transition from emeraldine to pernigraniline.[36] On the basis of the surrounded area of CV loop, a gradually increased current density with the increase of PANi incorporation revealed an improved specific capacitance as a result of significant contribution from reversible surface redox reaction between PANi and H_2SO_4 electrolyte. The pure PANi electrode, however, only exhibited a moderate current response, suggesting a low electrochemical utilization efficiency due to its very low surface area (63 m^2/g in Table 1). The galvanostatic charge−discharge curves of the composite electrodes at constant current density of 0.25 A/g are shown in Figure 6b. A typical triangular profile of the CMK-5 electrode revealed a dominated EDL charge storage mechanism, in good agreement with its rectangular CV curves (Figure 6a). However, the charge−discharge profile of the composite electrodes had two evident voltage stages, which is a combination of EDL capacitance with the pseudocapacitance. Nevertheless, the near symmetric charge and discharge curves reflect the fast ion adsorption/desorption on CMK-5 electrode and reversible Faradic redox reaction between PANi and H_2SO_4 electrolyte.

The single-electrode specific capacitances calculated from the discharge curves at constant current density of 0.1 A/g are summarized in Table 1. The CMK-5 electrode presented a specific capacitance of 293 F/g. This value is remarkably higher as compared with other carbon electrodes (normally in the range of 100−200 F/g), such as CMK-3,[30] conventional CMK-5,[37] and carbide-derived carbon electrode.[38] The extraordinarily high specific capacitance of platelet CMK-5 is attributed to its high surface area, bimodal mesopores, good electronic conductivity, and short ion diffusion pathway. These structural properties greatly promoted the ion and electron transports in the CMK-5 electrode, thus facilitating the formation of double-layer capacitance and improving the rate performance. The specific capacitance of CMK-5 was further improved by PANi incorporation. As shown in Table 1, the CMK-5-PANi composite electrodes exhibited a gradually increased specific capacitance with the increase of the PANi amount. A maximum specific capacitance of 803 F/g was achieved for CMK-5-PANi-64 composite electrode, a value significantly higher than those of pristine CMK-5 (293 F/g) and pure PANi electrode (629 F/g) (Table 1), suggesting a complementary synergetic effect between the two components. This effect enabled CMK-5-PANi-64 composite electrode to exhibit a more higher specific capacitance as compared with other carbon/PANi composite including graphene/PANi (200−480 F/g),[27,39,40] graphene/PANi film (640 F/g),[35] 3DOM/PANi (352 F/g),[24] mesoporous carbon CMK-3/PANi (470 F/g),[30] and HCS/PANi (525 F/g).[36] Given that the specific capacitance of PANi highly

dx.doi.org/10.1021/am4018016 | ACS Appl. Mater. Interfaces 2013, 5, 7501−7508

depends on the electrode loading, the device configuration as well as the calculation method,[23,41] the two-electrode configuration, and the high loading of working electrode in our work (5.0 mg in 1 cm^2 stainless steal mesh) allow us to believe that our measured specific capacitance is reliable in predicting its practical performance. Moreover, by assuming the capacitance of the composite coming from EDL capacitance of CMK-5 and pseudocapacitance of PANi, a simple calculation by deducting the contribution of CMK-5 from the composite yielded the specific capacitance of pure PANi (Table 1). A specific capacitance of 1090 F/g was calculated for PANi in CMK-PANi-64 composite. Considering its theoretical capacitance of 2000 F/g in H_2SO_4 aqueous electrolyte,[42] more than 50% PANi in the CMK-5-PANi-64 composite was involved in the surface redox reaction, highlighting the significant role of CMK-5 in improving the electrochemically active surface area of PANi by providing mesochannels for PANi nanoparticles and offering a large external surface area for coating of PANi thin films.

Figure 6c shows the Nyquist plots of supercapacitors fabricated symmetrically with different electrodes. For each electrode, its Nyquist plot consisted of a semicircle in the high-frequency region followed by a vertical line along the imaginary axis in the low-frequency region. The semicircle intercepted the real axis at R_s in the very high frequency region and at $R_s + R_{ct}$ in the high frequency region (inset in Figure 6c), corresponding to the electrolyte resistance (R_s) and charge transfer resistance (R_{ct}), respectively.[43,44] It is noted that the solution resistance was insensitive to electrode materials, while R_{ct} differed markedly from one electrode to another. The smallest R_{ct} of CMK-5 electrode can be explained by its good electronic conductivity and the straight and short mesochannels, which allowed for fast transport of electrolyte ions. In contrast, the R_{ct} of the composite electrodes showed a gradual increase with the increase in PANi content in the composites. These more resistive capacitive performances are in good agreement with the relatively low electronic conductivity of PANi and its kinetically slow surface redox reaction.[27] Moreover, the narrowed pore size due to the entry of PANi particles into the CMK-5 mesochannels may also slow the transport of electrolyte ion in the interior of electrode, resulting in a large diffusion resistance.

The dependence of IR drop with the current density for the symmetric supercapacitors is shown in Figure 6d. A simple calculation from the slope of voltage vs the current density yielded the ESR of a supercapacitor, and the results are given in Table 1. The ESR included the electronic resistance of the electrode, the diffusion resistance of ions in the nanopores of the electrode, and the interfacial contact resistance between the electrode and the current collector.[9,45] The large difference of ESR between pristine CMK-5 electrode (0.027 ohm) and pure PANi electrode (0.124 ohm) is closely related to their different charge storage mechanism. However, it is interesting to see that the ESR of composite electrodes only showed moderate increase from 0.034 to 0.050 ohm as PANi increased from 40 to 64 wt % in the composite. On the basis of these results, it is concluded that incorporating PANi to CMK-5 electrode not only affords much more active surface area for electrochemical redox reaction but also greatly improves the overall electronic conductivity for rapid charge transfer.

The IR drops of different electrode materials significantly affect their rate performances. As demonstrated in Figure 7a, with current density increase from 0.1 to 10 A/g, the CMK-5

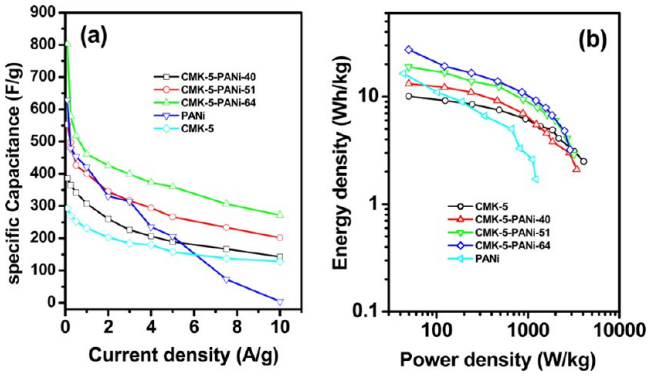

Figure 7. Variation of specific capacitance with current density for different electrode materials (a) and Ragone plots of a symmetric two-electrode supercapacitor (b). Data were obtained from the galvanostatic discharge process at current densities varying from 0.1 to 10 A/g.

electrode shows a capacitance decrease from 293 to 128 F/g. Such an excellent capacitance retention can be attributed to its straight and short mesochannels that could significantly promote ion transport in the interior of the electrode. However, due to relatively poor electronic conductivity and the predominate contribution of pseudocapacitance, pure PANi electrode shows a dramatic capacitance decay from initial value of 629 F/g at 0.1 A/g to almost zero at 10 A/g. It is interesting to see that incorporating PANi to CMK-5 can distinctly improve the overall rate performance of the composite electrode. Even at high discharge current density of 10 A/g, the CMK-5-PANi composite electrodes still maintain a specific capacitance of 143, 202, and 272 F/g, respectively, as 41, 51, and 64 wt % PANi were incorporated (Figure 7a). These results are much higher than 128 F/g of CMK-5 and 4 F/g of pure PANi electrode measured at an identical current density and thus suggests an improved rate performance of PANi by incorporation to the platelet CMK-5 carbon matrix.

Figure 7b shows the Ragone plots of supercapacitors configured with different symmetric electrodes. The energy density stored in a supercapacitor is expressed by $E = 1/2CV^2$, while the power density is expressed by $P = E/t$, where C is the total capacitance (F/g) measured from the two electrode system, V is the cell voltage (V) excluding IR drop, and t is the discharge time (s). The CMK-5-PANi composite electrode displays significantly improved capacitive performance as compared with PANi electrode. The pure PANi electrode delivers a moderate energy density of 16.4 Wh/kg at power density of 43 W/kg, but it drops quickly to 1.7 Wh/kg as the power density increases to 1227 W/kg. The poor power performance of PANi electrode is related to its low rate performance and large ESR (Table 1). In particular, the CMK-5-PANi-64 composite electrode delivers an energy density as high as 27.4 Wh/kg at a power density of 50 W/kg. This energy density is even higher than that of most of the asymmetric supercapacitors with a voltage window close to 2.0 V in aqueous electrolyte, for example, 26.3 Wh/kg of graphene-PANi/graphene-RuO_2 electrode,[46] 21.3 Wh/kg of MnO_2/graphene electrode,[47] 24.3 Wh/kg of MnO_2/aMEGO (activated microwave expanded graphite oxide),[48] and 23.2 Wh/kg of graphene hydrogel/MnO_2 array electrode.[49] Moreover, at high power density of 2900 W/kg, the CMK-5-PANi-64 electrode still remains at an energy density of 3.2 Wh/kg. Such remarkable capacitive behavior is suggested to be the

integration of the high rate performance of CMK-5 with the high pseudocapacitance of PANi.

The long-term cyclability of the CMK-5-PANi-64 composite in the voltage window of 0−1.0 V was measured by a consecutive galvanostatic charge−discharge at constant current density of 4.0 A/g (Figure 8). The CMK-5 electrode shows an excellent electrochemical stability with 98% capacitance retention after 1000 cycles measurement, which is the essential nature of EDL capacitors. In contrast, a capacitance retention of only 68% was observed for pure PANi electrode. This poor cyclability is presumably related to its large particles that may undergo continuous swelling and shrinkage during the charging−discharging process. It is interesting to see that this severe volume change can be largely avoided by incorporation to platelet CMK-5. It is noted that the CMK-5-PANi-64 composite electrode exhibits a substantially improved electrochemical stability with 81% capacitance retention after 1000 cycles. The nearly symmetric charge and discharge curves of the last 10 cycles (Figure S2, Supporting Information) and the similar CV profiles before and after 1000 cycles (Figure S3, Supporting Information) reveal the high reversibility and good electrochemical stability of the composite electrode. The small PANi particles confined in the mesochannles of CMK-5 and its thin film on external surface of CMK-5 would offer a high electrochemically active surface area for Faradic redox reaction, while the CMK-5 carbon matrix with straight and short mesochannels allows for the rapid electron and ion propagation within the electrode.

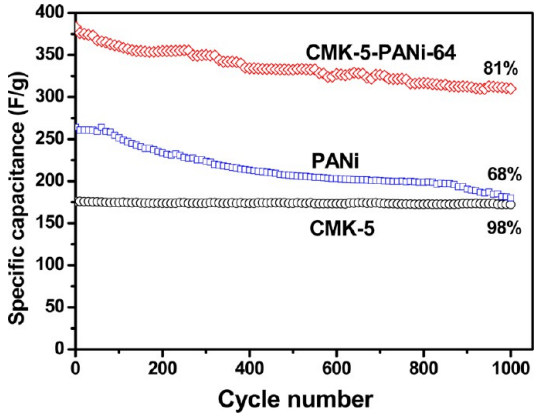

Figure 8. Cycling performance of supercapacitor with symmetric electrode of platelet CMK-5, PANi, and CMK-5-PANi-51 composite at a constant current density of 4.0 A/g in 2.0 mol/L aqueous H_2SO_4 electrolyte.

4. CONCLUSION

Platelet CMK-5 is a promising mesoporous carbon material for improvement of pseudocapacitance of PANi due to its unique properties, such as bimodal pore system, high surface area, and short ion diffusion pathway. PANi was found to be confined in the mesochannels as small particles and coated on the external surface of CMK-5 as its loading amount was increased, thus significantly improving the electrochemically active area available for Faradic redox reactions. Specific capacitance as high as 803 F/g and energy density as high as 27.4 Wh/kg were achieved with a composite electrode containing 64 wt % PANi (CMK-PANi-64). In contrast, pure CMK-5 and PANi electrodes delivered capacitances and energy densities of 293 and 629 F/g and 10.1 and 16.4 Wh/kg, respectively. Moreover, the CMK-5-PANi-64 electrode exhibited an excellent rate capability and a substantially improved electrochemical stability with 81% capacitance retention after 1000 continuous charge−discharge cycles. The excellent capacitive behavior of the CMK-5-PANi composite electrode is benefited from physicochemical properties of each component. The CMK-5 with good electric conductivity and open mesochannels allows for fast electronic and ion propagations, while PANi particles confined in the mesopores and thin films coated on the external surface of CMK-5 maximize the surface area available for redox reactions. Such composite electrodes consisting of mesoporous carbon and conducting polymer represent one of the promising candidates for high-performance supercapacitors.

■ ASSOCIATED CONTENT

Supporting Information

Small-angle XRD patterns of platelet CMK-5 and CMK-5-PANi composite, the last 10 cycles of galvanostatic charge−discharge, and the CV profile before and after 1000 cycles for CMK-5-PANi symmetric supercapacitor. This information is available free of charge via the Internet at http://pubs.acs.org

■ AUTHOR INFORMATION

Corresponding Author

*E-mail: zblei@snnu.edu.cn (Z. Lei); george.zhao@uq.edu.au (X.S. Zhao). Tel: 86-29-81530810 (Z. Lei); +61-7-33469997 (X.S. Zhao). Fax: 86-29-81530702 (Z. Lei); +61-7-33654199 (X.S. Zhao).

Notes

The authors declare no competing financial interest.

■ ACKNOWLEDGMENTS

This work was supported by the National Nature Science Foundations of China (Grant No. 51172137), Fundamental Research Funds for the Central Universities (Grant Nos.: GK201102002, GK201101003, GK201301002), and the Starting Funds of Shaanxi Normal University. Australian Research Council (ARC) is acknowledged for funding projects FT100100879 and DP130101870.

■ REFERENCES

(1) Miller, J. R.; Simon, P. *Science* **2008**, *321*, 651−652.
(2) Simon, P.; Gogotsi, Y. *Nat. Mater.* **2008**, *7*, 845−854.
(3) Lee, S. W.; Gallant, B. M.; Byon, H. R.; Hammond, P. T.; Shao-Horn, Y. *Energy Environ. Sci.* **2011**, *4*, 1972−1985.
(4) Zhang, J.; Zhao, X. S. *ChemSusChem* **2012**, *5*, 818−841.
(5) Simon, P.; Gogotsi, Y. *Acc. Chem. Res.* **2013**, *46*, 1094−1103.
(6) Zhang, L. L.; Zhao, X. S. *Chem. Soc. Rev.* **2009**, *38*, 2520−2531.
(7) Wang, G.; Zhang, L.; Zhang, J. *Chem. Soc. Rev.* **2012**, *41*, 797−828.
(8) Jiang, H.; Lee, P. S.; Li, C. *Energy Environ. Sci.* **2013**, *6*, 41−53.
(9) Lei, Z. B.; Christov, N.; Zhao, X. S. *Energy Environ. Sci.* **2011**, *4*, 1866−1873.
(10) Lu, X.; Zhai, T.; Zhang, X.; Shen, Y.; Yuan, L.; Hu, B.; Gong, L.; Chen, J.; Gao, Y.; Zhou, J.; Tong, Y.; Wang, Z. L. *Adv. Mater.* **2012**, *24*, 938−944.
(11) Li, Q.; Wang, Z.-L.; Li, G.-R.; Guo, R.; Ding, L.-X.; Tong, Y.-X. *Nano Lett.* **2012**, *12*, 3803−3807.
(12) Lang, X.; Hirata, A.; Fujita, T.; Chen, M. *Nat. Nanotechnol.* **2011**, *6*, 232−236.
(13) Liu, J.; Jiang, J.; Cheng, C.; Li, H.; Zhang, J.; Gong, H.; Fan, H. J. *Adv. Mater.* **2011**, *23*, 2076−2081.

(14) Wu, Z.-S.; Zhou, G.; Yin, L.-C.; Ren, W.; Li, F.; Cheng, H.-M. *Nano Energy* **2012**, *1*, 107−131.
(15) Zhang, L. L.; Xiong, Z.; Zhao, X. S. *J. Power Sources* **2013**, *222*, 326−332.
(16) Dong, X.-C.; Xu, H.; Wang, X.-W.; Huang, Y.-X.; Chan-Park, M. B.; Zhang, H.; Wang, L.-H.; Huang, W.; Chen, P. *ACS Nano* **2012**, *6*, 3206−3213.
(17) Saravanakumar, B.; Purushothaman, K. K.; Muralidharan, G. *ACS Appl. Mater. Interfaces* **2012**, *4*, 4484−4490.
(18) Shao, M.; Ning, F.; Zhao, Y.; Zhao, J.; Wei, M.; Evans, D. G.; Duan, X. *Chem. Mater.* **2012**, *24*, 1192−1197.
(19) Li, D.; Huang, J. X.; Kaner, R. B. *Acc. Chem. Res.* **2009**, *42*, 135−145.
(20) Kumar, N. A.; Choi, H.-J.; Shin, Y. R.; Chang, D. W.; Dai, L.; Baek, J.-B. *ACS Nano* **2012**, *6*, 1715−1723.
(21) Yan, Y.; Cheng, Q.; Pavlinek, V.; Saha, P.; Li, C. *Electrochim. Acta* **2012**, *71*, 27−32.
(22) Niu, Z.; Luan, P.; Shao, Q.; Dong, H.; Li, J.; Chen, J.; Zhao, D.; Cai, L.; Zhou, W.; Chen, X.; Xie, S. *Energy Environ. Sci.* **2012**, *5*, 8726−8733.
(23) Wang, Y.; Yang, X.; Qiu, L.; Li, D. *Energy Environ. Sci.* **2013**, *6*, 477−481.
(24) Zhang, L. L.; Li, S.; Zhang, J. T.; Guo, P. Z.; Zheng, J. T.; Zhao, X. S. *Chem. Mater.* **2010**, *22*, 1195−1202.
(25) Woo, S.-W.; Dokko, K.; Nakano, H.; Kanamura, K. *J. Power Sources* **2009**, *190*, 596−600.
(26) Wu, Q.; Xu, Y. X.; Yao, Z. Y.; Liu, A. R.; Shi, G. Q. *ACS Nano* **2010**, *4*, 1963−1970.
(27) Wang, D. W.; Li, F.; Zhao, J. P.; Ren, W. C.; Chen, Z. G.; Tan, J.; Wu, Z. S.; Gentle, I.; Lu, G. Q.; Cheng, H. M. *ACS Nano* **2009**, *3*, 1745−1752.
(28) Zhang, H.; Cao, G.; Wang, Z.; Yang, Y.; Shi, Z.; Gu, Z. *Electrochem. Commun.* **2008**, *10*, 1056−1059.
(29) Mondal, S. K.; Barai, K.; Munichandraiah, N. *Electrochim. Acta* **2007**, *52*, 3258−3264.
(30) Yan, Y.; Cheng, Q.; Wang, G.; Li, C. *J. Power Sources* **2011**, *196*, 7835−7840.
(31) Li, L.; Song, H.; Zhang, Q.; Yao, J.; Chen, X. *J. Power Sources* **2009**, *187*, 268−274.
(32) Lei, Z. B.; Liu, Z.; Wang, H.; Sun, X.; Lu, L.; Zhao, X. S. *J. Mater. Chem. A* **2013**, *1*, 2313−2321.
(33) Hulicova-Jurcakova, D.; Puziy, A. M.; Poddubnaya, O. I.; Suárez-García, F.; Tascón, J. M. D.; Lu, G. Q. *J. Am. Chem. Soc.* **2009**, *131*, 5026−5027.
(34) Lei, Z. B.; Bai, S. Y.; Xiao, Y.; Dang, L. Q.; An, L. Z.; Zhang, G. N.; Xu, Q. *J. Phys. Chem. C* **2008**, *112*, 722−731.
(35) Feng, X.-M.; Li, R.-M.; Ma, Y.-W.; Chen, R.-F.; Shi, N.-E.; Fan, Q.-L.; Huang, W. *Adv. Funct. Mater.* **2011**, *21*, 2989−2996.
(36) Lei, Z. B.; Chen, Z. W.; Zhao, X. S. *J. Phys. Chem. C* **2010**, *114*, 19867−19874.
(37) Lei, Z. B.; Bai, D.; Zhao, X. S. *Microporous Mesoporous Mater.* **2012**, *147*, 86−93.
(38) Rose, M.; Korenblit, Y.; Kockrick, E.; Borchardt, L.; Oschatz, M.; Kaskel, S.; Yushin, G. *Small* **2011**, *7*, 1108−1117.
(39) Zhang, K.; Zhang, L. L.; Zhao, X. S.; Wu, J. *Chem. Mater.* **2010**, *22*, 1392−1401.
(40) Wu, Q.; Xu, Y.; Yao, Z.; Liu, A.; Shi, G. *ACS Nano* **2010**, *4*, 1963−1970.
(41) Stoller, M. D.; Ruoff, R. S. *Energy Environ. Sci.* **2010**, *3*, 1294−1301.
(42) Li, H.; Wang, J.; Chu, Q.; Wang, Z.; Zhang, F.; Wang, S. *J. Power Sources* **2009**, *190*, 578−586.
(43) Lei, Z. B.; Shi, F.; Lu, L. *ACS Appl. Mater. Interfaces* **2012**, *4*, 1058−1064.
(44) Biswas, S.; Drzal, L. T. *Chem. Mater.* **2010**, *22*, 5667−5671.
(45) Lei, Z. B.; Zhang, J.; Zhao, X. S. *J. Mater. Chem.* **2012**, *22*, 153−160.
(46) Zhang, J.; Jiang, J.; Li, H.; Zhao, X. S. *Energy Environ. Sci.* **2011**, *4*, 4009−4015.
(47) Deng, L.; Zhu, G.; Wang, J.; Kang, L.; Liu, Z.-H.; Yang, Z.; Wang, Z. *J. Power Sources* **2011**, *196*, 10782−10787.
(48) Zhao, X.; Zhang, L.; Murali, S.; Stoller, M. D.; Zhang, Q.; Zhu, Y.; Ruoff, R. S. *ACS Nano* **2012**, *6*, 5404−5412.
(49) Gao, H.; Xiao, F.; Ching, C. B.; Duan, H. *ACS Appl. Mater. Interfaces* **2012**, *4*, 2801−2810.